Guiding thermomagnetic avalanches with soft magnetic stripes

V. K. Vlasko-Vlasov, F. Colauto, T. Benseman, D. Rosenmann, and W.-K. Kwok

Guiding thermo-magnetic avalanches with soft magnetic stripes

V. K. Vlasko-Vlasov[1] , F. Colauto[1,2] , T. Benseman[1,3] , D. Rosenmann[4] , W.-K. Kwok[1]

[1] Materials Sciences Division, Argonne National Laboratory
[2] Federal University of Sao Carlos, Brazil
[3] City University of New York, CUNY Queens College
[4] Center for Nanomaterials, Argonne National Laboratory

We demonstrate the potential for manipulating the ultrafast dynamics of thermo-magnetic flux avalanches (TMA) in superconducting films with soft magnetic stripes deposited on the film. By tuning the in-plane magnetization of the stripes, we induce lines of strong magnetic potentials for Abrikosov vortices, resulting in guided *slow* motion of vortices along the stripe edges and preferential *bursts* of TMA along the stripes. Furthermore, we show that transversely polarized stripes can reduce the TMA size by diverting magnetic flux away from the major trunk of the TMA into inter-stripe gaps. Our data indicate that TMAs are launched from locations with enhanced vortex entry barrier, where flux accumulation followed by accelerated vortex discharge significantly reduces the threshold of the applied field ramping speed required for the creation of TMAs. Finally, vortex-antivortex annihilation at the moving front of an expanding TMA can account for the enhanced TMA activity in the receding branches of the sample's magnetization cycle and the preferred propagation of TMAs into maximum trapped flux regions.

I. Introduction

Magnetic flux jumps or thermo-magnetic avalanches (TMAs), is a common phenomenon in hard superconductors (see reviews [1- 3]). These TMAs interrupt the continuous flow of supercurrents and abruptly break down the Bean critical state, resulting in a sharp reduction of the magnetization in bulk and thin film superconductors (SC). The irreproducibility and unpredictability of the flux jumps can cause sporadic oscillations of the magnetic moment [4-11], appearance of large electromagnetic noise [12-13], and can even lead to physical destruction of the samples [14-15]. Due to these negative effects, TMAs are considered detrimental to SC applications, which stimulated numerous efforts to promote their mitigation by nanostructuring of the SC samples or interlacing them with Foucault damping metal layers.

In this work, we accentuate a positive aspect of TMAs, namely their unique extremely fast dynamics, with flux propagation speeds reaching up-to 180 km/s in $YBa_2Cu_3O_{7-d}$ [16] and 360 km/s in YNi_2B_2C films [17]). Such a remarkable speed, exceeding the Larkin-Ovchinnikov limiting velocity for magnetic flux vortices [18] by orders of magnitude, can be a very attractive feature for the creation of principally new ultrafast vortex devices, if the nucleation and evolution of flux avalanches could be strictly controlled.

Various attempts have been made to manipulate TMAs using periodic arrays of nanoholes or magnetic nanodots [19-22], depositing metal layers on top of a superconductor [23-26], modulating the thickness of the SC film [27], constructing multilayered architectures of SC stripes [28], irradiating SC films [29] and forming

indentations at the film edge [30-31]. These studies showed that extending branches of dendritic shaped TMAs in SC films can be partially directed along symmetry axes of the patterned defect arrays and surface steps, or can be deflected from their initial direction upon entry under a capping metal layer. However, the degree of TMA control was substantially limited. Below, we describe a potentially more efficient way to manipulate TMAs in superconducting films using thin narrow stripes of soft ferromagnetic material to guide flux motion. The magnetic potential of the stripes is tunable and forces TMA propagation along the stripe edges, suppresses branching of the TMAs, and under certain conditions can produce gates for launching TMAs.

II. Experiment

Our samples consist of squares of 100 nm thick niobium (Nb) film with arrays of thin permalloy (Py) stripes deposited on top. The Nb film was sputtered using high-vacuum magnetron system into four 2x2 mm squares silhouetted on a 1x1 cm² silicon substrate by laser lithography. After lift-off, the Nb squares were covered with a 10 nm thick layer of SiO_2 to avoid proximity effects. Next, 35 µm wide stripes of 40 nm thick Py film separated by 2 to 5 µm gaps were deposited onto the center of two of the Nb squares, 200µm away from the square edges, using e-beam lithography and a lift-off process. The large width and the small thickness of the stripes were chosen to warranty their in-plane magnetization and to clearly distinguish the flux density variations near their edges. In turn, relatively wide bare Nb film area allows clear comparison of of the vortex dynamics in the regions with and without Py stripes.

On the third sample, the ends of the stripes were extended to the edge the Nb film. The fourth Nb square was left pristine as a reference sample. The substrate was then diced into four individual samples. Furthermore, one of the two Nb squares with centered Py pattern, was obliquely cut, so that the ends of the Py stripes terminated at a sharp angle. This feature allowed us to reveal some peculiar effects of the enhanced stray fields at the sharp stripe corners as described below. Our thin Py stripes have planar magnetic anisotropy with a coercivity of a few Gauss, allowing in-plane polarization in a desired direction with the application of a small in-plane magnetic field.

The magnetic flux entry and exit from our samples under slowly varying external magnetic fields applied *normal* to the film was visualized using a magneto-optical imaging system [32] coupled with a closed cycle helium optical cryostat (Montana Instruments) operating below the critical temperature of our Nb film (T_c= 8.7 K). To magnetize the Py stripes, the samples were cooled in the presence of an in-plane field (75 to 150 Oe) along, across, or at 45^0 to the stripes, which remained fixed during the measurement. On a 100 nm thick reference Nb sample without Py stripes, we checked that an in-plane field up-to ~1 kOe does not affect vortices normal to the film [36]. At a chosen temperature, T < T_c, a field, H_a, was applied normal to the film in small steps of ~1 Oe at a rate of $\dot{H}_a$ ~0.5 Oe/sec. At each step, a magneto-optical image of the flux distribution was obtained within ~30 seconds (with ~0.1 s exposure time). During this time the field was not changing and was incremented with the same slow rate only after image acquisition. At H_a > 50 Oe, when for T>3.1K, TMAs cease to nucleate at our slow rates, the field step was increased to ~5 Oe and the field ramp rate was doubled. After reaching the maximum field of ~300 Oe, which is several times larger than the total penetration field at 3.1K, the field, H_a, was ramped down

by reversing the above procedure. The typical slow flux dynamics in our Py/Nb hybrid structures is described in detail in recent publications [33-35]. Here, we present the low temperature observations of the emergence and development of TMAs with different polarization of the Py stripes on our Nb films, and demonstrate control of their dynamics.

II. TMA patterns in Nb films with Py stripes

The smooth entry and exit of vortices at temperatures $T > T_c/2$, in our samples can be strongly modified by changing the polarization of the Py stripes on top of the Nb film (see details in [33-35]). The manipulation of flux dynamics is due to the tunable attraction/repulsion of vortices to the edges of the Py stripes. These vortex-edge interactions change with in-plane magnetization **M** of the stripes, which determines the strength of the induced edge magnetic charges, ρ_M=-div**M**. Maximum charge density along the longitudinal Py stripe edge is reached when the in-plane magnetic moments are perpendicular to this edge. ρ_M will be positive or negative, depending on the polarity of **M** and the charge density per unit edge length will be σ_m=2Md (where d is the thickness of the film with a sharp vertical edge). If **M** is parallel to the stripe, ρ_M=0, and the effect of the longitudinal edges becomes negligible. For Abrikosov vortices generated by an applied normal field, the magnetically charged edges of the Py stripe form attractive channels or repulsive barriers depending on the sign of ρ_M with respect to the vortex polarity, resulting in rapid guided penetration or retardation of vortices. Therefore, by rotating the in-plane field and changing the magnetic charges along the long and short edges of the Py stripes, one can realize a 'magnetic triode' behavior for Abrikosov vortices, entering from the sample boundaries, similar to electron flow manipulation in an electronic triode [33] .

Thermo-magnetic avalanches or TMAs appear at $T \lesssim T_c/2$ as commonly observed in Nb samples [30, 37-41]. These avalanches are highly reproducible in successive runs under the same conditions. They tend to burst into the sample from specific sample perimeter points and form dendritic flux patterns that can propagate along and across the Py stripes. These nucleation points are probably associated with accidental defects formed during sample manufacturing. The following evolution and the shape of the dendrites strongly depend on the magnetization of the Py stripes. Below, we illustrate changes in the TMA behavior for different orientations of the in-plane magnetization field.

The sequence of images in Fig.1a-d depicts TMA jumps in the sample with *longitudinally* polarized Py stripes (an in-plane field of 150 Oe is along white arrow in Fig.1a), where the magnetic charges form only at the stripe ends while the longitudinal edges remain neutral. For this sample, the Py stripes (35 μm wide with 5 μm gaps) are 200 μm away from the edges of the Nb square film as shown in the schematic in Fig. 1. First, the sample is cooled to T=3.3K in the above mentioned in-plane field. Then a magnetic field,H_a, normal to the sample plane, is ramped up to a maximum value of + or -280 Oe. At this temperature, no TMAs appear during the initial field ramp. Upon decreasing the magnetic field, a single avalanche (Fig.1b and 1d) consistently jumps near the bottom right edge of the film, independent of the polarity of H_a. The TMA propagates along the diagonals of the square where $|B_z|$ has local maximum (bright and dark diagonal lines in Fig.1a and Fig.1c). Such TMA activity while ramping down the field and tendency to travel along the maximum trapped flux regions are general features that we observe in all our samples, including the

reference Nb film shown in Fig.1e. This behavior was also reported for other superconducting films (e.g. [42]) and was allegedly associated with a minimum flux density requirement for the nucleation of a TMA that is satisfied only during the descending branch of the magnetization loop. We will discuss our understanding of this effect below.

When the in-plane field is rotated perpendicular to the Py stripes (transverse polarization), strong magnetic charges are induced along the long edges of the stripes. This essentially modifies the vortex dynamics by opening channels for easy vortex propagation along the stripe edges, while forming barriers for lateral vortex motion across the stripes, thereby introducing a strong supercurrent anisotropy (see Fig. 2a and ref. [33-35]). The transverse polarization of the stripes reduces the temperature of the appearance of TMAs. At the lowest temperature of ∼3.1 K, we still observe TMAs with dendritic shapes. With decreasing H_a, these TMAs can now nucleate from different locations (see Fig.2b and c). The general features of TMAs traveling along regions of locally highest trapped vortex density remains the same but the shape of the dendritic patterns change. The width of the TMA dendrites decreases upon their propagation into the sample and secondary branches are diverted towards the Py stripe edges. However, at this lowest temperature, the effect of Py stripes on TMA is relatively weak. It becomes much stronger with increasing temperature when the magnetically charged stripe edges become more efficient in altering the TMA branching structure. To illustrate this effect, we show a TMA pattern in a sample with *diagonally* polarized Py stripes at 4K (Fig.3). The charge density, ρ_M, at the stripe edges is $1/\sqrt{2}$ of that in the transversely polarized stripes, but is enough to totally align the secondary TMA branches parallel to the Py stripes. The dark branches expanding from the main TMA trunk along the stripes in Fig.3b appear similar to the slower flux instabilities (marked by short arrows in Fig.3a) arising from the inhomogeneous supercurrent anisotropy induced by the edges of the Py stripes (see [34]).

For transversely polarized Py stripes at T=3.4K, this effect is more pronounced, as shown in Fig. 4, where we present an expanded view of a top-left quarter of another sample. Here, several TMAs jump across the stripes from a nucleation spot formed at a small break in the Nb film edge (black arrow in Fig. 4a). Unlike at lower temperatures and in the sample presented in Fig. 2, here, the TMAs nucleate already during the initial ramping up of the normal field. Each trunk of the TMA becomes a source for secondary flux branches that travel along the longitudinal Py stripe edges for some distance. The escape of flux from the TMA trunk stunts the growth of the TMA and reduces its power. In contrast, the TMA dynamics is not affected by longitudinally polarized Py stripes (Fig.4b).

Fig.5 shows the entire sample with transversely and longitudinally polarized Py stripes in decreasing fields. The TMAs appear at the same location as in Fig.4, but for both stripe polarizations, they are noticeably larger than those launched during the initial field application. As in Fig.4a for the transversely polarized case, the magnetic charges at the stripe edges align the secondary branches and deplete flux from the main TMA trunk, thus diminishing the entire magnetic avalanche (smaller area and reduced number of branches in TMA of Fig.5a as compared to 5b). Again, we observe the decreasing width of the TMA dendrite (shrinking length of the vertically aligned vortex branches) as the TMA travels deeper into the sample. The resulting fir tree-like shape of the TMA in Fig.5a, compared with the widening TMA for the longitudinal stripe polarization in Fig.5b, confirms the progressive attenuation of the TMA traversing under the transversely polarized stripes.

An important feature of the sample illustrated in Fig.4 and Fig.5 is the extension of the Py stripes to the bottom of the sample. The overlap of the Py stripes with the edge of the Nb square film lowers the geometrical edge barrier in the case of transversely polarized stripes and promotes the easy vortex entry from this edge, channeling them along the inter-stripe gaps. This reduces the current and field concentration at the bottom edge, thereby suppressing the nucleation of TMAs. For longitudinal polarization of the Py stripes (Fig.5b), the effect of stripes at this Py/Nb overlapping edge is not visible and does not depend on the sign of the magnetic charge at the stripe ends. This indicates that the magnetic potential induced at the stripe ends where they overlap with the Nb film edge is relatively small compared to the geometrical barrier which restricts the flux entry in superconducting films (see details in [35]).

The situation changes dramatically in the sample where the Py stripes overlap with the edge, which is cut at an oblique angle as shown in Figures 6 and 7 for longitudinally and transversely polarized Py stripes, respectively. Fig.6a shows a schematic of the Bean critical state for the longitudinally polarized Py stripes. The critical current density (distance between the current lines) is the same over the entire sample except at the top ends of the Py stripes. For the in-plane polarization direction of the Py stripes shown by the long arrow in Fig.6b, the top ends of the stripe at 200 μm from the Nb film edge, form barriers for the motion of positive (bright contrast in Fig.6b-e) flux such that the supercurrent is locally increased. At the bottom side of the sample, the Py stripes terminate at the Nb film edge, but unlike in the sample shown in Fig.5 they have triangular-shaped ends. The sharp angle of the terminated Py stripes generate concentrated magnetic stray fields, which can promote the launch of TMAs. Roughly, compared to the linear magnetic charges at the transversely polarized stripe edges where the stray fields decay as $1/r$ with distance r from the edge, the sharp corners act as point charges with the field diverging as $1/r^2$ near the corner.

When the stripes are polarized longitudinally, the TMA dendrites jump from these launch points both with the initial field application and during decreasing field from maximum., Although as in the previous examples, the TMAs appear more active with decreasing field. Figure 6 shows a series of successive TMA images observed at 4K with field reduction from H_a=280 Oe. The TMAs originate exclusively from the oblique cut bottom edge of the sample and propagate perpendicular to this edge in accordance with direction of the Lorentz force produced by the supercurrents schematically shown in Fig.6a. New TMA dendrites predominantly jump between previous TMAs into areas with local maximum of the residual flux. This can be easily seen from the comparison of e.g. Fig.6d and e, where we mark the TMAs by numbers corresponding to their successive appearance. Here, TMA 4 and 5 in Fig.6e jump between TMA 1 and 2, followed by TMA 6 entering between TMA 4 and 1. However, at large flux density, a new TMA can randomly overrun the previous patterns (compare Fig.6e and f). The flux jumps diminish at larger fields, as is usually observed in SC films and bulk samples. With further increasing field, the smooth flux entry from the all sample edges wipes out the dendritic TMA patterns and restores the typical critical state picture (Fig.6h-k).

For transversely polarized Py stripes, the overall critical state picture in the sample with the oblique cut edge is qualitatively similar to that of the longitudinally polarized stripes. Although, lines of sharp current turns (blue lines schematically shown in Fig.7b), usually aligned with the diagonals of the sample corners and yielding local maximum of the

trapped flux (lines of bright contrast in Fig.7a), now shift due to the emerging critical current anisotropy induced by the transversely polarized Py stripes. Similar to the square sample with Py stripes overlapping the Nb film edge (Fig.5), the transverse polarization of the stripes initiates an advanced entry of vortices into the interstripe gaps from the bottom side. The TMAs also launch from this side and their branches are clearly aligned with the stripes. As in the previous examples, the TMA jumps occur more actively on field reduction at low temperatures. However, in this case, the TMAs strictly follow the interstripe gaps after nucleating at the bottom of the sample and transverse branching occurs mostly near the center of the sample where the currents change sign (horizontal bright line in Fig. 7a). In different cycles of remagnetization, at decreasing positive or negative field, the TMA patterns are very similar (compare Fig.7 (c-d) and (e- f)). The TMA patterns marked in Fig.7 (d) and (f) as "new" confirm that successive TMAs jump into regions between previous TMAs where the trapped flux density has local maximum. Finally, comparison of Figs. 6 and 7 shows that in the sample with transversely polarized Py stripes, the TMAs occur much less frequently than in the longitudinally polarized sample. This is consistent with the observed advanced vortex entry along the inter-stripe gaps, which should relax the field concentration at the sample edges.

In addition to the fast TMAs, in the case of transversely polarized stripes, we observe slower flux jumps (marked "FI" in Fig.7e) that form narrow antivortex strips (in this case bright contrast) along the stripes. The development of FI, extending fast from the edge to the middle of the sample, could be noticed by eye unlike that of the "instant" TMA jumps. However, it was not resolved with minimum 20 ms exposure time of our camera. These slower flux jumps are associated with a dynamic instability caused by strongly inhomogeneous anisotropic magnetic potential induced by charged stripe edges. A possible reason preventing them from transforming into well developed TMAs is the smaller initial speed of vortices entering across a relaxed edge barrier.

In the initial critical state with transversely polarized Py stripes (Fig.7a-b), the supercurrents typically flow along the sides of the sample. However, when a flux jump occurs, the current flow is interrupted by the TMA where the critical current drops to zero, resulting in current trajectories circumventing the TMA area. With further increasing field, new vortices enter from the sample edges, smoothing over the TMA pattern and restoring the initial current trajectories. Eventually, the flux and current distribution returns to the critical state structure similar to that in Fig.7a.

The main results of our observations can be summarized as follows:
1) When Py stripes are polarized *longitudinally*, they hardly affect the appearance of TMA in a square sample, indicating that possible additional heat sink and Foucault damping introduced by thin 40 nm Py stripes are minor compared to other factors responsible for the flux jumps. This is regardless of whether the short ends of the Py stripes extend to the Nb film edge or terminate at some distance away from it.
2) When a side of a sample with the Py stripes extending to the Nb film edge is cut at an oblique angle, leaving sharp edge with triangular Py stripe ends, the concentrated stray fields of the triangular ends in the case of the *longitudinal* stripe polarization, essentially assist in the nucleation of TMAs.

3) In the case of *transversely polarized* Py stripes, the lines of induced magnetic charges along the long stripe edges promote flux depletion from the central TMA trunk through the escape of vortices into inter-stripe gaps and progressively reduce the size of the TMA.

4) *Transversely polarized* Py stripes overlapping with the Nb film edge partially suppress the nucleation of TMA by facilitating easy vortex entry along gaps between the Py stripes.

5) In the sample with the an oblique cut edge, *transversely polarized* Py stripes induce linear TMA patterns along the stripes.

6) For all cases, the TMA activity is noticeably higher on the descending branches of the remagnetization cycle compared with the initial field application. New TMAs jump between previously formed TMAs into regions with maximum residual flux of opposite polarity.

7) For low TMA density, the avalanches repeatedly start from the same preferred launching points at the sample perimeter.

III. Discussion

The nature of thermo-magnetic flux jumps in superconductors was recognized long ago [4-6]. It was attributed to the emergence of flux dynamics instability when local heating due to the energy dissipation of moving vortices is generated faster than its diffusion inside the sample and in the environment. The critical state, where vortices pinned on defects yield flux gradients equilibrated by the critical current, is intrinsically metastable and tends to decay even though spontaneous relaxation times can be astronomically long [43]. However, the relaxation can occur extremely fast, in the form of avalanche bursts, if the system is perturbed by adding or removing vortices. This happens at large enough electric fields induced above a ramping rate threshold of the magnetic field, which strongly perturb the smooth redistribution of vortices through flux creep. The term "flux avalanche" is a direct analogy to mountain avalanches, where shaken critical snow masses rush down steep slopes while accumulating weakly pinned deposits along the way.

Modern computer capabilities allow simulation of various scenarios for the structure and time evolution of the TMAs in SC films with different geometries and pinning site distributions (see recent works [44-46] and references there) revealing intricate, system dependent dendritic flux patterns. These simulations are based on the combined solution of the nonlinear *macroscopic* thermal and magnetic diffusion equations. The thermal balance accounts for the electric field E generated by the changing magnetic flux $\dot{B}$ that results in energy dissipation, EJ, by the supercurrent J, which causes local heating released into the sample body, substrate, and coolant. In turn, the magnetic flux diffusion is described by the Maxwell equations using different approximations for the E-J material laws [47-52]. In bulk samples, the shielding supercurrents are described by the local gradients of induction. However, in the case of films, one has to account for the integral (nonlocal) magnetic flux-current relations. An important factor is the choice of random or structured defects [19-20, 53-57]. They affect the branching patterns of the TMA [45, 51, 55, 58-61] even though the threshold for dendritic flux jumps in films is usually defined by *macroscopic* parameters, including magnetic and thermal diffusion coefficients, the value and ramping speed of the magnetic field, temperature, and sample dimensions [51, 58]. The simulated complex flux patterns are remarkably similar to the TMA dendritic patterns observed in many experiments.

The main condition for the TMA is a small ratio τ of the magnetic flux diffusion time t_M and the heat diffusion time t_{TH}. When the driven flux motion is much faster than the thermal relaxation ($\tau \ll 1$), then the local temperature along the vortex trajectory increases, facilitating an easy pathway and acceleration for subsequent vortices to follow, leading to a flux avalanche.

In bulk materials, $t_M \sim L^2/D_M$, and $t_{TH} \sim L^2/D_{TH}$, with magnetic and thermal diffusion coefficients $D_M=\mu_0/\rho$, $D_{TH}= \kappa/C$, and a diffusion distance L [1]. Hence, $\tau_b=\mu_0\kappa/\rho C$. Here, ρ is the resistivity (estimates often use the flux flow resistivity ρ_{FF} or the normal state resistivity ρ_n at T_c), κ is the heat conductivity, and C is the heat capacity.

However, in superconducting films of thickness, d, the magnetic diffusion is nonlocal (due to integral field-current relations), resulting in $t_M \sim L_h d/D_M$ and $t_{TH} \sim L_h^2/D_{TH}$ [51]. Here, the thermal diffusion length $L_h=(d\kappa/h)^{1/2}$ accounts for the heat transfer to the substrate with a transfer coefficient h. Hence, $\tau=\tau_b d/L_h$ can be much smaller than in bulk samples. For Nb films with d=100nm, using coefficients $\kappa \simeq 0.2$ W/cm, $h \simeq 1$W/cm²K, $\rho_n \simeq 3\times 10^{-7}$ Ω cm, $C \simeq 2\times 10^{-3}$ J/cm³ K at ~4.2K [51], we find $\tau \sim 0.045$, which explains the high probability of TMA occurrence in our samples. The estimated thermal diffusion length, $L_h \sim 13$ μm, gives an approximate width of the TMA filaments. It is smaller than the cross section of the base TMA trunks but close to the width of the secondary branches emanating from the TMA trunks in Figs. 1-7. In principle, the secondary branches retracting vortices along the Py strips could evolve later with a slower speed compared to the main TMA stamp. However, the resulting reduced size of the TMAs, defined by the progressive loss of the flux, points that the major vortex escape along the stripes happens during the time of the TMA propagation.

The threshold for the field ramping speed, where the dispersion relations for the instability allow rapidly growing excitations with a finite wavelength, i.e. the launch of branching TMA, is [51]:

$$\dot{B}_c = hJ_1\beta_c/dbJ_c|\partial J_c/\partial T| \quad , \text{with } \beta_c=[(1+2q^2)^{1/2} + q(1+1/s)^{1/2}]^2 \quad, \text{and } q=\pi/2(b/L_h)$$

All the terms here are in real physical units. J_1 is a coefficient in the current-electric field relation J(E), $J_c(T)$ is the temperature dependent critical current, $s=E/\rho J$, and b is the flux penetration distance at an applied field B. Using the creep formula $J(E)=J_c+J_1\ln(E/E_0)$ approximated by $J=J_c(E/E_0)^{1/n}$ with $n=J_c/J_1 \gg 1$, and $1/\rho = \partial J/\partial E=J_1/E \sim J_c/n$, such that $s=J_c/nJ$, and assuming $J \sim J_c$, we have $s \sim 1/n=J_1/J_c$. The following estimates are obtained using typical values of n=20 and 60.

From our data on the flux entry distance, *b*, at different fields and temperatures for pure Nb film, we estimate J_c(4K)~4×10^{10}A/M², and $\partial J_c/\partial T$~1.1×10^{10} A/M²K. Here, we used the formula for long, superconducting strips of width 2w [62, 63]: $H_a=(J_cd/\pi)\text{arccosh}[w/(w- b)]$. It gives a reasonable approximation for our square sample for sufficiently short *b*. Then β_c(4K)~2.5 at n=20 and β_c~3.9 at n=60 for the field H_a=10 Oe when we observe the first TMA during initial field ramp. The resulting threshold field ramp rates $\dot{B}_c$ ~3×10^3 T/s at n=60 and $\dot{B}_c$ ~6×10^3 T/s at n=20 are much larger than the experimental values. The same discrepancy was found in [58] where it was associated with the local nucleation of TMA. Despite the slowly changing macroscopic field, small vortex bundles can jump extremely fast in some local spots, yielding very large electric fields $E \sim \dot{B}$

capable of launching an avalanche. Note that in recent simulations [44-45] based on the existing macroscopic theory, the ramp rates required for realization of TMAs are in the range of hundreds of T/s.

Our findings are consistent with the local nucleation of TMA and we assume that it is regulated by individual spots at the superconducting film perimeter, where vortices enter through enhanced edge barriers that essentially exceed bulk pinning. The local magnetic pressure in these spots can accumulate due to increased local current density, until vortices break though the barrier and move much faster than in neighboring spots, thus nucleating a TMA. The observation of repeated launches of TMA from the same location during different field runs validates our assumption.

When the entry of vortices around the enhanced barrier spot is alleviated by transversely polarized Py stripes that promote easy vortex channeling, the magnetic field concentration drops and reduces the probability of the flux jumps. This explains the absence of TMAs at the bottom side of the sample with transversely polarized stripes overlapping the Nb film edge in Fig.5. Also, such a scenario can explain the reduction of TMA activity for the transversely polarized sample cut at an oblique angle (Fig.7) compared to the case of the longitudinal polarization (Fig.6). At the same time, the enhanced frequency of TMA in Fig.6 compared to other our samples, is due to the effect of concentrated magnetic stray fields at the triangular stripe ends and due to the sharply cut edge of the Nb film. In samples fabricated using the lift-off technique, the edges of the Nb film are relatively smooth. However, the oblique bottom side of the sample in Fig.6-7 has a sharp vertical cut, forming a stronger barrier for vortex entry. The smooth edge of the Nb film result in the total absence of TMAs when the stripes are transversely polarized (Fig.5). However, in the sample with the sharply cut edge, the TMA activity does not vanish even for transversely polarized stripes (Fig.7) revealing the importance of the edge barrier for TMA nucleation. So far, there were no observations of TMAs launched from points inside the samples, and all published experimental results report TMA nucleation at the sample edges. Obviously, accounting for the locally enhanced edge barrier is necessary for an adequate treatment of TMA.

A clear feature of the flux jumps in our samples, which is observed also in other superconducting films (e.g. [30, 42]), is the enhanced TMA activity during field reduction. This can be associated with the annihilation of vortices (V) trapped after application of the initial field and antivortices (AV) carried by the TMA launched upon decreasing H_a. The V-AV annihilation should locally release a considerable amount of energy ($E_r \sim 2\varepsilon_v d$ for each V-AV pair, where ε_v is the unit length vortex energy). The resulting increased temperature at the advancing V-AV front will assist the TMA propagation towards the largest annihilation (highest T) direction, i. e. into regions with largest trapped vortex density. In addition, the preferential TMA jumps into regions between previously generated TMA pathways and into regions with densely trapped vortices should be supported by the AV-AV repulsion and V-AV attraction. Interestingly, simulations of TMA in films with partially trapped flux [64] based on macroscopic flux description, also show such a tendency. In that case, the anti-flux flow into regions of high flux density seems to be regulated by the local enhancement of $\dot{B}$ ($\sim$ E) at the TMA front, which should be transformed into local heating, EJ. However, the direct account of the released V-AV annihilation energy at the front could yield even stronger effect on the vortex motion and decrease the $\dot{B}$ threshold for TMA.

IV. Conclusions

In this work, we demonstrated the potential for manipulating fast moving thermomagnetic flux avalanches in superconducting samples using thin, soft ferromagnetic stripes deposited on their surface. By rotating the in-plane magnetization of the stripes, we can tune the magnetic potential at the stripe edges, and control the vortex dynamics in the underlying superconducting film to change the frequency, size, and structure of the TMAs. The transversely polarized Py stripes induce channels for the easy vortex motion, extracting vortices from the expanding TMA into inter-stripe gaps, thereby successively shrinking the width of the TMA and reducing its total area. When the transversely polarized Py stripes overlap with the superconducting Nb film edge, they relax the field concentration at the edge by promoting easy vortex entry, and reduce the probability of TMA nucleation. At the same time, the launched TMAs in this case transform into single line structures aligned with the stripes rather than evolve into the typical dendritic patterns.

In addition to the effect of stripes, we analyzed conditions for TMA nucleation and showed that existing theoretical models yield threshold field ramping speeds for launching TMAs that greatly exceed experimental values. We suggest that this discrepancy can be resolved by taking into consideration locally enhanced edge barrier, which can promote very fast initial velocity of confined vortex bundles in particular spots at the sample perimeter.. In addition, direct inclusion of the vortex-antivortex annihilation at the TMA front should be included in the theory to explain the increased activity of flux jumps in the descending branches of the remagnetization cycles.

Our ferromagnetic/superconducting hybrid structures enable control of vortex avalanches in superconducting films and demonstrate its potential for novel electronic devices based on ultrafast flux motion.

References

[1] R. G. Mints and A. L. Rakhmanov, Rev. Mod. Phys. **53**, 551 (1981). **Critical state stability in type-II superconductors and superconducting-normal-metal composites**.

[2] S. L. Wipf, Cryogenics **31**, 936 (1991). **Review of stability in high temperature superconductors with emphasis on flux jumping**.

[3] E. Altshuler and T. H. Johansen, Rev. Mod. Phys. **76**, 471 (2004). **Colloquium: Experiments in vortex avalanches**.

[4] S. L. Wipf and M. S. Lubell, Phys. Lett. 16, 103 (1965). **Flux jumping in Nb-25% Zr under nearly adiabatic conditions**.

[5] S.L. Wipf, Phys. Rev. 161, 404 (1967). **Magnetic Instabilities in Type-II Superconductors**.

[6] P. S. Swartz and C. P. Bean, J. Appl. Phys. **39**, 4991 (1968). **A Model for Magnetic Instabilities in Hard Superconductors: The Adiabatic Critical State**.

[7] S. X. Dou, X. L. Wang, J. Horvat, D. Milliken, A. H. Li, K. Konstantinov, E. W. Collings, M, D, Sumption, H. K. Liu, Physica C **361**, 79 (2001). **Flux jumping and a bulk-to-granular transition in the magnetization of a compacted and sintered MgB2 superconductor**.

[8] Z. W. Zhao, S. L. Li, Y. M. Ni, H. P. Yang, Z. Y. Liu, H. H. Wen, W. N. Kang, H. J. Kim, E. M. Choi, S. I. Lee, Phys. Rev. B **65**, 064512 (2002). **Suppression of superconducting critical current density by small flux jumps in MgB2 thin films**.

[9] E. M. Choi, H. S. Lee, H. J. Kim, S. I. Lee, H. J. Kim, W. N. Kang, Appl. Phys. Lett. **84**, 82 (2004). **Enhancement at low temperatures of the critical current density for Au-coated thin films**.

[10] T. H. Johansen, M. Baziljevich, D. V. Shantsev, P. E. Goa, Y. M. Galperin, W. N. Kang, H. J. Kim, E. M. Choi, M.-S. Kim, and S. I. Lee, Europhys.Lett. 5 9, 599 (2002). **Dendritic magnetic instability in superconducting MgB2 films**.

[11] V. Chabanenko, V. Rusakov, V. Yampolskii, S. Vasiliev, A. Nabialek, H. Szymczak, S. Piechota, O. Mironov, J. Low Temp. Phys. **130**, 165-174 (2003). **The Structure of Magnetic Avalanches: Experiment and Model for Avalanche Vortex Matter Penetration**.

[12] G. Mohler, D. Stroud, Phys. Rev. B **60**, 9738 (1999). **Flux noise resulting from vortex avalanches using a simple kinetic model**

[13] R. Eggenhoffner, E. Celasco, V. Ferrando, M. Celasco, Appl. Phys. Lett. **86**, 022504 (2005). **Vortex avalanche phenomena in MgB2 superconducting film studied by current noise measurements**.

[14] P. Brull, D. Kirchgassner, P. Leiderer, P. Berberich, H. Kinder, Annal. Der Phys. 1, 243 (1992). **Magnetic-field-induced damage in a superconducting YBa2Cu3O7-x film**.

[15] S. Gruss , G. Fuchs, G. Krabbes, P. Verges, G. Stover, K. H. Muller, J. Fink, L. Schultz, Appl. Phys. Lett. **79**, 3131 (2001). **Superconducting bulk magnets: Very high trapped fields and cracking**.

[16] U. Bolz, B. Biehler, D. Schmidt, B. U. Runge, P. Leiderer , Europhys. Lett. **64**, 517 (2003). **Dynamics of the dendritic flux instability in YBa2Cu3O7-delta films**.

[17] B. Biehler, B. U. Runge, S. C. Wimbush, B. Holzapfel, P. Leiderer, Supercond. Sci. Technol. **18**, 385 (2005). **Velocity measurements of the dendritic instability in YNi2B2C**.

[18] A. I. Larkin and Yu. N. Ovchinnikov, Zh. Eksp. Teor. Fiz. 68, 1915 (1975) [Sov. Phys.-JETP 41, 960 (1976)]. **Nonlinear conductivity of superconductors in the mixed state**.

[19] V. Vlasko-Vlasov, U. Welp, V. Metlushko, and G. W. Crabtree, Physica C **341–348**, 1281 (2000). **Flux avalanches in superconducting films with periodic arrays of holes**.

[20] M. Menghini, R. J. Wijngaarden, A. V. Silhanek, S. Raedts, V.V. Moshchalkov, Phys. Rev. B **71**, 104506 (2005). **Dendritic flux penetration in Pb films with a periodic array of antidots**.

[21] D. G. Gheorghe, R. J. Wijngaarden, W. Gillijns, A. V. Silhanek, and V. V. Moshchalkov. Phys. Rev. B **77**, 054502 (2008). **Magnetic flux patterns in superconductors deposited on a lattice of magnetic dots: A magneto-optical imaging study**.

[22] M. Motta, F. Colauto, J. I. Vestgarden, J. Fritzsche, M. Timmermans, J. Cuppens, C. Attanasio, C. Cirillo, V. V. Moshchalkov, J. Van de Vondel, T. H. Johansen, W. A. Ortiz, A. V. Silhanek, Phys. Rev. B **89**, 134508 (2014). **Controllable morphology of flux avalanches in microstructured superconductors**.

[23] J. Albrecht, A. T. Matveev, M. Djupmyr, G. Schutz, B. Stuhlhofer, H. U. Habermeier, Appl. Phys. Lett. 87, 182501 (2005). **Bending of magnetic avalanches in MgB$_2$ thin films.**

[23b] F. Colauto, E. J. Patino, M. G. Blamire and W. A. Ortiz, Supercond. Sci. Technol. **21,** 045018 (2008). **Boundaries of the instability region on the HT diagram of Nb thin films**.

[24] F. Colauto, E. Choi, J. Y. Lee, S. I. Lee, E. J. Patino, M. G. Blamire, T. H. Johansen, W. A. Ortiz, Appl. Phys. Lett. **96**, 092512 (2010). **Suppression of flux avalanches in superconducting films by electromagnetic braking**.

[25] J. Brisbois, B. Vanderheyden, F. Colauto, M. Motta, W. A. Ortiz, J. Fritzsche, N. D. Nguyen, B. Hackens, O.-A. Adami and A. V. Silhanek, New J. Phys. **16**, 103003 (2014). **Classical analogy for the deflection of flux avalanches by a metallic layer**.

[26] P. Mikheenko, T. H. Johansen, S. Chaudhuri, I. J. Maasilta, I. J. & Y. M. Galperin, Phys. Rev. B **91**, 060507 (2015). **Ray optics behavior of flux avalanche propagation in superconducting films**.

[27] J. Brisbois, V. N. Gladilin, J. Tempere, J. T. Devreese, V. V. Moshchalkov, F. Colauto, M. Motta, T. H. Johansen, J. Fritzsche, O.-A. Adami, N. D. Nguyen, W. A. Ortiz, R. B. G. Kramer, A.

V. Silhanek, Phys. Rev. B **95**, 094506 (2017). **Flux penetration in a superconducting film partially capped with a conducting layer**.

[28] T. Tamegai, A. Mine, Y. Tsuchiya, S. Miyano, S. Pyon, Y. Mawatari, S. Nagasawa, M. Hidaka, Physica C **533,** 74 (2017). **Critical states and thermomagnetic instabilities in three-dimensional nanostructured superconductors**.

[29] D. Barness, M. Sinvani, A. Shaulov, T. Tamegai, Y. Yeshurun, Phys. Rev. B 77, 094514 (2008). **Finger patterns of magnetic flux in bulk Bi2Sr2CaCu2O8+delta samples**.

[30] J. Brisbois, O.-A. Adami, J. I. Avila, M. Motta, W. A. Ortiz, N. D. Nguyen, P. Vanderbemden, B. Vanderheyden, R. B. G. Kramer, and A. V. Silhanek, Phys. Rev. B **93**, 054521 (2016). **Magnetic flux penetration in Nb superconducting films with lithographically defined microindentations**.

[31] D. Carmo, F. Colauto, A. M. H. de Andrade, A. A. M. Oliveira, W. A. Ortiz and T. H. Johansen, Supercond. Sci. Technol. **29**, 095003 (2016). **Controllable injector for local flux entry into superconducting films**.

[32] V. K. Vlasko-Vlasov, U. Welp, G. W. Crabtree, and V. I. Nikitenko, NATO ASI Ser. E: Appl. Sci. **356**, 205 (1999). **Magneto-optical studies of magnetization processes in high-Tc superconductors**.

[33] V. K. Vlasko-Vlasov, F. Colauto, T. Benseman, D. Rosenmann, and W.-K. Kwok, Sci. Rep. **6**, 36847 (2016). **Triode for magnetic flux quanta**.

[34] V. K. Vlasko-Vlasov, F. Colauto, A. I. Buzdin, D. Rosenmann, T. Benseman, and W.-K. Kwok, Phys. Rev. B **95**, 144504 (2017). **Magnetic gates and guides for superconducting vortices**.

[35] V. K. Vlasko-Vlasov, F. Colauto, A. I. Buzdin, D. Rosenmann, T. Benseman, and W.-K. Kwok, Phys. Rev. B **95**, 174514 (2017). **Manipulating Abrikosov vortices with soft magnetic stripes**.

[36] V. K. Vlasko-Vlasov, F. Colauto, A. I. Buzdin, D. Carmo, A. M. H. Andrade, A. A. M. Oliveira, W. A. Ortiz, D. Rosenmann, and W.-K. Kwok, Phys. Rev. B **94**, 184502 (2016). **Crossing fields in thin films of isotropic superconductors**.

[37] W. DeSorbo and W. A. Healy, Cryogenics **4**, 257-323 (1964). **The intermediate state of some superconductors**.

[38] M. R. Wertheimer and J. le G. Gilchrist, J. Phys. Chem Sol. **28**, 2509 (1967). **Flux jumps in type II superconductors**.

[39] P. L. Gammel, R. E. Miller, and D. J. Bishop, Phys. Rev. B **52**, 75 (1995). **Observation of magnetic-field penetration via dendritic growth in superconducting niobium films**.

[40] F. Colauto, J. I. Vestgarden, A. M. H. de Andrade, A. A. M. Oliveira, W. A. Ortiz, T. H. Johansen, Appl. Phys. Lett. **103**, 032604 (2013). **Limiting thermomagnetic avalanches in superconducting films by stop-holes**.

[41] J. I. Vestgarden, F. Colauto, A. M. H. de Andrade, A. A. M. Oliveira, W. A. Ortiz, T. H. Johansen, Phys. Rev. B **92**, 144510 (2015). **Cascade dynamics of thermomagnetic avalanches in superconducting films with holes**.

 [42] S. C. Wimbush, B. Holzapfel, C. Jooss, J. Appl. Phys. **96**, 3589 (2004). **Observation of dendritic flux instabilities in YNi2B2C thin films**.

[43] A. Gurevich, Int. J. Mod. Phys. B **9**, 1045 (1995). **Nonlinear flux diffusion in superconductors**.

[44] Z. Jing, H. Yong and Y. Zhou, Supercond. Sci. Technol. **29**, 105001 (2016). **Influences of non-uniformities and anisotropies on the flux avalanche behaviors of type-II superconducting films**.

[45] Z. Jing, H. Yong, Y. Zhou, J. Appl. Phys. **121**, 023902 (2017). **Numerical simulation on the flux avalanche behaviors of microstructured superconducting thin films**.

[46] J. I. Vestgarden, Y. M. Galperin, T. H. Johansen, Phys. Rev. B **93**, 174511 (2016). **Oscillatory regimes of the thermomagnetic instability in superconducting films**.

[47] E. H. Brandt, Phys. Rev. B **52**, 15442 (1995). **Electric field in superconductors with rectangular cross section**.

[48] A. Gurevich, E. H. Brandt, Phys. Rev. B **55**, 12706 (1997). **ac response of thin superconductors in the flux-creep regime**.

[49] R. G. Mints, E. H. Brandt Phys. Rev. B **94**, 12421 (1996). **Flux jumping in thin films**.

[50] A. L. Rakhmanov, D. V. Shantsev, Y. M. Galperin, and T. H. Johansen, Phys. Rev. B **70**, 224502 (2004). **Finger patterns produced by thermomagnetic instability in superconductors**.

[51] I. S. Aranson, A. Gurevich, M. S. Welling, R. J. Wijngaarden, V. K. Vlasko-Vlasov, V. M. Vinokur, and U. Welp, Phys. Rev. Lett. **94**, 037002 (2005). **Dendritic flux avalanches and nonlocal electrodynamics in thin superconducting films**.

[52] D. V. Shantsev, A. V. Bobyl, Y. M. Galperin, T. H. Johansen, and S. I. Lee, Phys. Rev. B **72**, 024541 (2005). **Size of flux jumps in superconducting films**.

[53] T. Tamegai, Y. Tsuchiya, Y. Nakajima, T. Yamamoto, Y. Nakamura, J. S. Tsai, M. Hidaka, H. Terai, Z. Wang, Physica C 470, 734 (2010). **Preferential diagonal penetration of vortices into square superconducting networks**.

[54] M. Motta, F. Colauto, R. Zadorosny, T. H. Johansen, R. B. Dinner, M. G. Blamire, G. W. Ataklti, V. V. Moshchalkov, A. V. Silhanek, and W. A. Ortiz, Phys. Rev. B 84, 214529 (2011). **Visualizing the ac magnetic susceptibility of superconducting films via magneto-optical imaging**.

[55] R. Zadorosny, F. Colauto, M. Motta, T. H. Johansen, R. Dinner, M. Blamire, G. W. Ataklti, V. V. Moshchalkov, A. V. Silhanek, W. A. Ortiz, J. Supercond. Nov. Magn. **26**, 2285 (2013). **Morphology of Flux Avalanches in Patterned Superconducting Films**.

[56] M. Motta , F. Colauto , W. A. Ortiz , J. Fritzsche , J. Cuppens , W. Gillijns , V. V. Moshchalkov , T. H. Johansen , A. Sanchez , and A. V. Silhanek , Appl. Phys. Lett. **102** , 212601 (2013). **Enhanced pinning in superconducting thin films with graded pinning landscapes**.

[57] M. Motta, F. Colauto, J. I. Vestgarden, J. Fritzsche, M. Timmermans, J. Cuppens, C. Attanasio, C. Cirillo, V. V. Moshchalkov, J. Van de Vondel, T. H. Johansen, W. A. Ortiz, A. V. Silhanek, Phys. Rev. B **89**, 134508 (2014). **Controllable morphology of flux avalanches in microstructured superconductors**.

[58] D.V. Denisov, D.V. Shantsev, Y. M. Galperin, E.-M. Choi, H.-S. Lee, S.-I Lee,[3]A.V. Bobyl, P. E. Goa, A. A. F. Olsen, and T. H. Johansen, Phys. Rev. Lett. **97**, 077002 (2006). **Onset of dendritic flux avalanches in superconducting films**.

[59] S. Treiber, C. Stahl, G. Schutz, and J. Albrecht, Phys. Rev. B **84**, 094533 (2011). **Stability of the current-carrying state in nonhomogeneous MgB2 films**.

[60] V. V. Yurchenko, K. Ilin, J. M. Meckbach, m. Siegel, A. J. Oliver, Y. M. Galperin, T. H. Johansen, Appl. Phys. Lett. **102**, 252601 (2013). **Thermo-magnetic stability of superconducting films controlled by nano-morphology**.

[61] J. I. Vestgarden, D. V. Shantsev, Y. M. Galperin, T. H. Johansen, Supercond. Sci. Technol. **26**, 055012 (2013). **The diversity of flux avalanche patterns in superconducting films**.

[62] E. H. Brandt and M. Indenbom, Phys. Rev. B **48**, 12893 (1993). **Type-II-superconductor strip with current in a perpendicular magnetic field**.

[63] E. Zeldov, J. R. Clem, M. McElkesh and M. Darwin, Phys. Rev. B **49**, 9802 (1994). **Magnetization and transport currents in thin superconducting films**.

[64] J. I. Vestgarden, P. Mikheenko, Y. M. Galperin, and T. H. Johansen, New J. Phys. **15**, 093001 (2013). **Nonlocal electrodynamics of normal and superconducting films**.

Figures
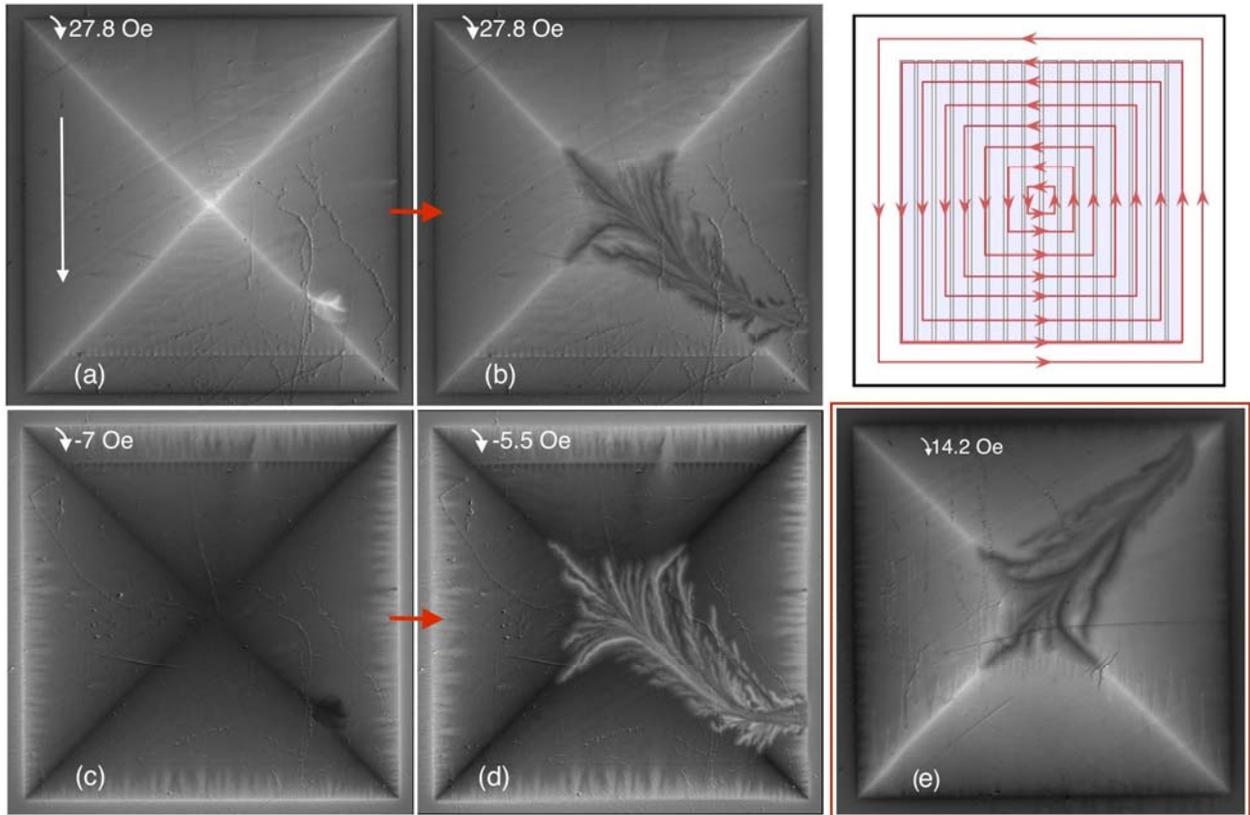

Fig.1 Magneto-optical image of Thermo-Magnetic-Avalanche (TMA) upon field reduction from $|H_a|$=280 Oe at T=3.3K in the case of longitudinally polarized Py stripes. Sample size is 2x2 mm. The polarization direction is shown by white arrow in (a). 35µm wide Py stripes with 5 µm gaps are deposited in the middle of a 2x2 mm 100nm thick Nb square at 200 µm away from the edges. In (a-b) the field is reduced from a maximum of H_a= +280 Oe, and in (c-d) from H_a = -280 Oe, to the values shown in the panels. (a) and (c) –depict the isotropic critical states. Note the line of enhanced current (increased contrast) along the ends of the stripes (above the bottom sample side in (a-b) and below top side in (c-d) (see details in [34-35]). The circulating current scheme corresponding to (a) is shown in the right-top panel. In (a) and (d), TMAs carrying antivortices jump at different field cycles from the same spot at the sample edge and advance along regions with local maximum density of trapped vortices (bright and dark diagonal lines in (a) and (c), respectively). (e) shows TMA in the reference Nb film without Py stripes at 3.4K (the field is reduced from H_a = +280 Oe).
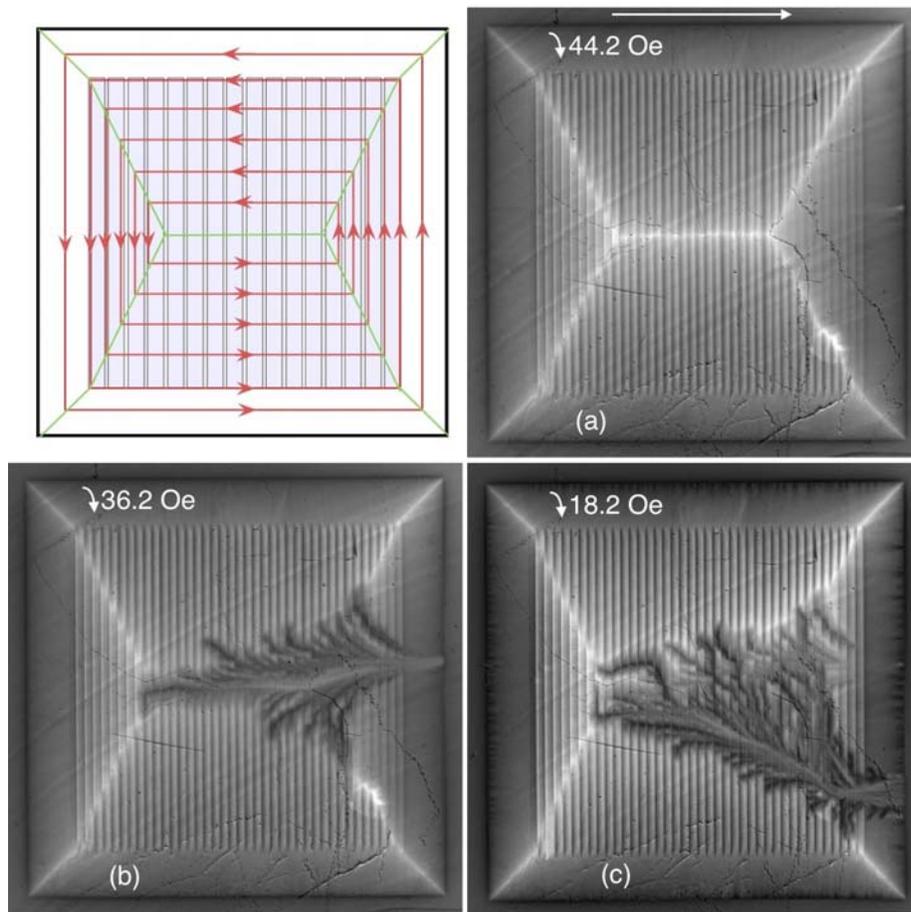
Fig.2 Consecutive TMA jumps at T=3.1K in the case of transversely polarized stripes for the same sample as in Fig.1. Sample size is 2x2 mm. The field is reduced from H_a = +280 Oe to the values shown in the panels. (a) Schematic of the critical state with isotropic J_c at the periphery and anisotropic J_c in the area with Py stripes. Note the kink in the diagonal bright lines at the corners of the Py stripe pattern. The direction of the stripe magnetization is shown by the long white arrow in (a). Dark contrasted dendritic TMAs in (b-c) extend preferentially into regions with locally maximum trapped flux (bright lines in (a)). At this lowest temperature, the effect of stripes on the shape of the TMA is relatively weak.
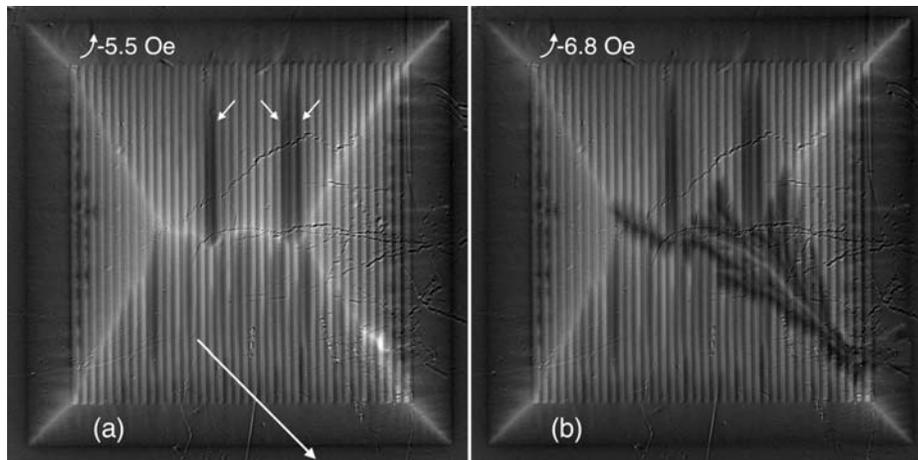
Fig.3 TMA in the same sample as in Fig.1-2 with diagonally polarized stripes at T=4K. Sample size is 2x2 mm. After application of +280 Oe the field was decreased to zero, and the negative H_a increases as shown on the panels. The stripe polarization is along white arrow shown in (a). The secondary dendritic branches in (b) stretch along the stripes. Short white arrows in (a) point to dark lines of slower flux instabilities arising from the inhomogeneous current anisotropy induced by the stray fields at the stripe edges.
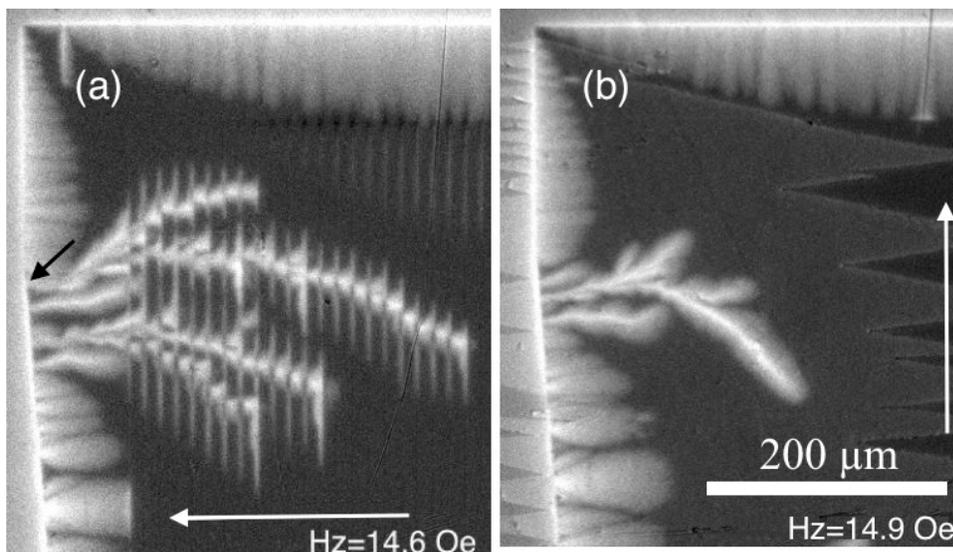
Fig.4 Expanded view of TMAs occurring with initial ramping of H_a on sample with (a) transversely and (b) longitudinally polarized stripes (polarization directions are shown by long white arrows) at T=3.4K. The stripes are 30 μm wide and have 2μm gaps. H_a is increased after zero field cooling to the values shown in the panels. In (a), TMAs jumping across the transversely polarized Py stripes spread vortices along the inter-stripe gaps and acquire a modulated structure. Black arrow in (a) points to a break at the left sample edge, which facilitates launching of the TMA. Above the break point the Nb film edge is rounded during sputtering into the lithographic pattern. Below the that point the broken Nb film has sharp edge with rectangular cross section which provides stronger barrier for the vortex entry.
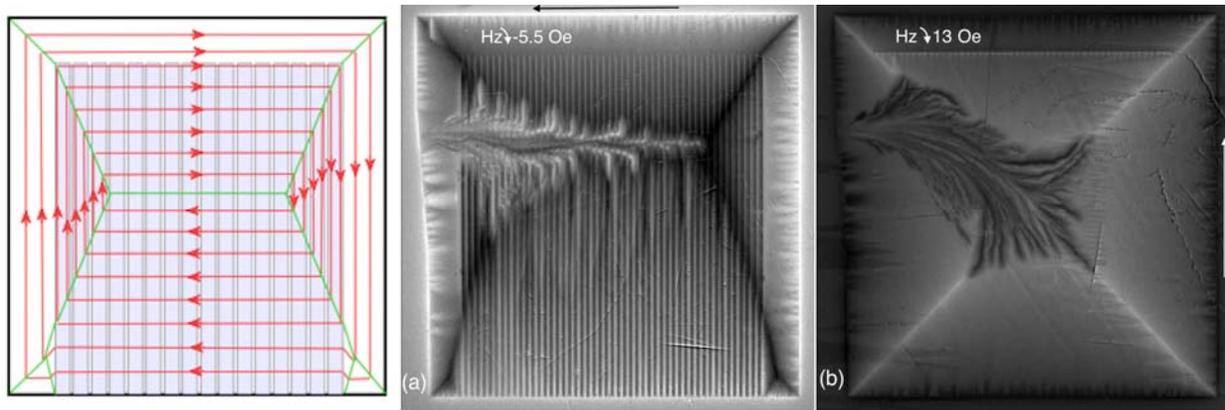
Fig.5 Entire image of TMA in the sample of Fig.4 with transversely (a) and longitudinally (b) polarized Py stripes at T=3.4K. Sample size is 2x2mm. Left panel shows the current scheme of the critical state in the case of transversely polarized Py stripes. In (a) the field is reduced from H_a=-280 Oe and in (b) from H_a=+280 Oe. TMAs jump from the same point into regions with maximum trapped flux (darkest areas in (a) and brightest in (b)). The total dendritic-shaped area is smaller for the transversely polarized stripes and the width of the TMA decreases with distance from the edge. In contrast, the TMA expands towards the end for the longitudinally polarized stripes. In (a) the Py stripes overlapping with the bottom edge of the Nb film provide easy vortex entry along the transversely polarized stripes (see [35] for details), which releases the magnetic pressure and suppresses flux instabilities at this edge.
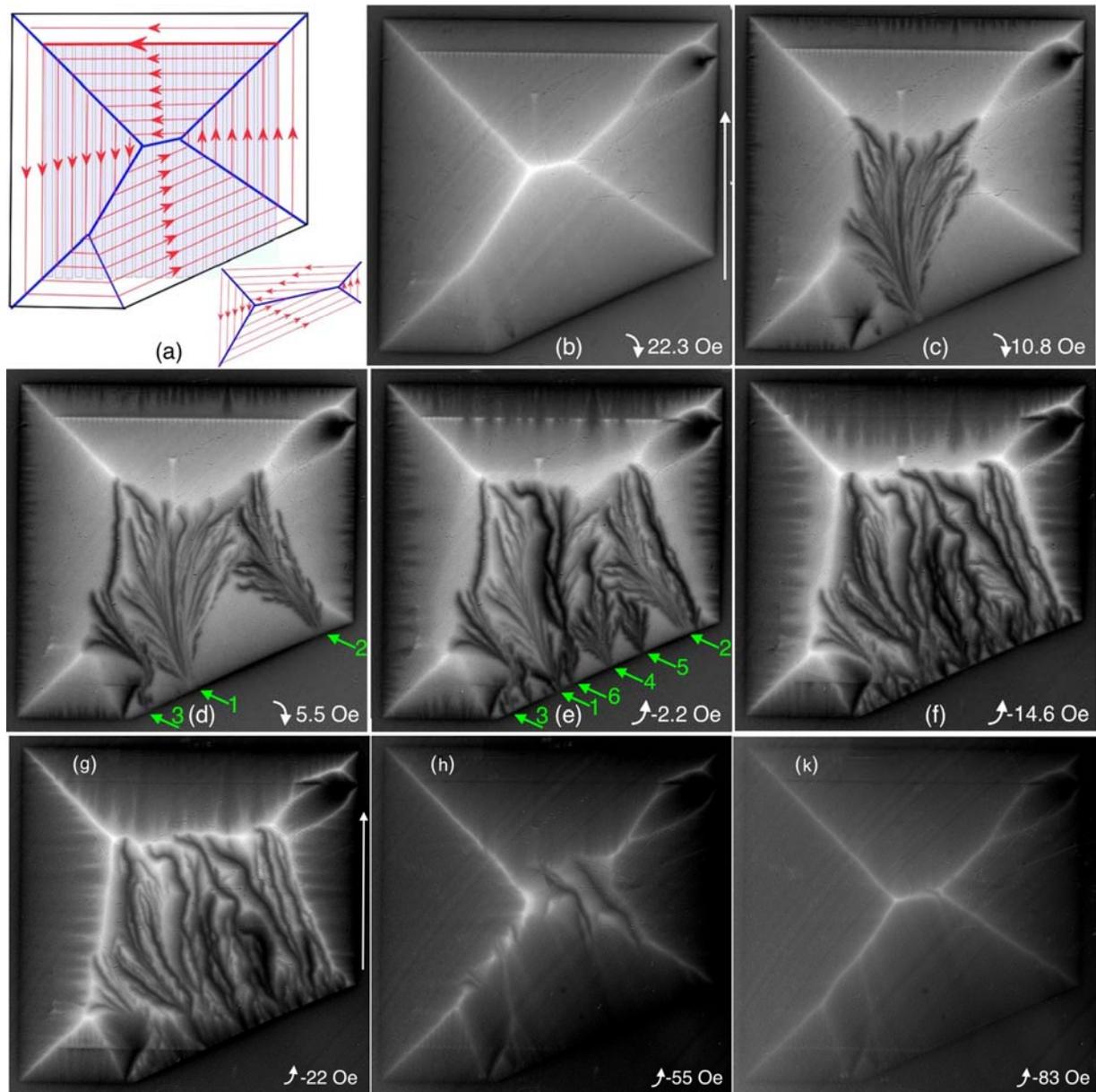
Fig.6 Successive TMA nucleation at T=4K in a sample with bottom side cut at an oblique angle. 30 μm wide stripes with 2 μm gaps are parallel to the vertical sample sides and are polarized longitudinally along the vertical arrow shown in (b). Sample width is 2 mm. (a) The schematic of the critical state corresponding to (b). Enlarged central part is shown on the bottom right of (a). The circulating supercurrents are isotropic and enhanced along the line of short stripe ends near the top side. New TMAs jump predominantly from the bottom side between previously formed TMAs. Successive TMA jumps, are indicated by arrows with corresponding numbers, from 1 to 6, in (d) and (e). With increasing the density of TMAs, new TMAs may override prior TMAs. (h-k) illustrate the healing process of the critical state with increasing negative magnetic field.
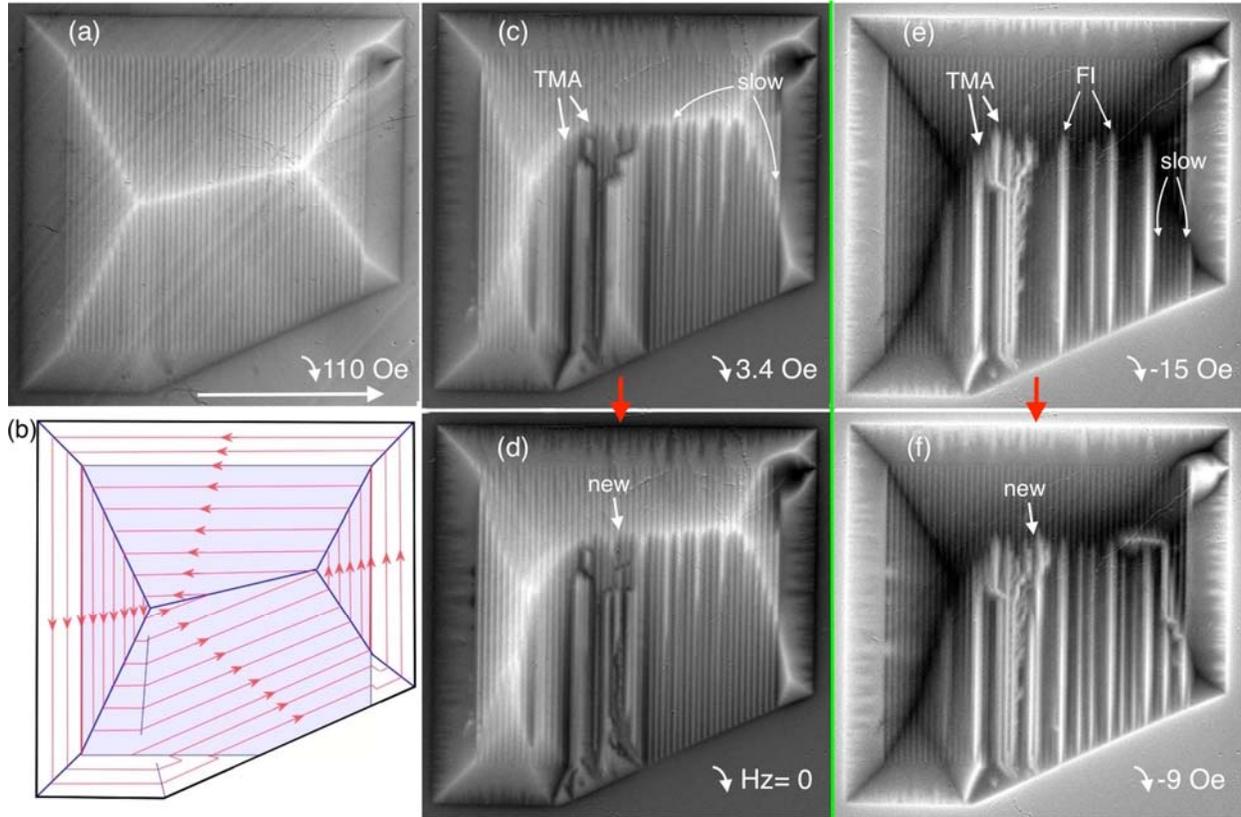
Fig.7 TMA at T=4K in the sample with obliquely cut edge and transversely polarized stripes. Sample width is 2 mm. (a) The critical state after reducing field from H_a=+280 Oe. (b)-current scheme for (a). (c-d) and (e-f) show successive TMA jumps (their tails are marked as "TMA") at reducing field from +280 Oe and -280 Oe respectively. Subsequent TMAs (marked "new") jump into regions with local maximum of the trapped flux (see red arrows from (c) to (d) and from (e) to (f)). In addition to TMAs there are lines of fast instabilities marked as FI in (e). The development of FI, fast extending from the edge to the middle of the sample, could be noticed by eye but was not resolved with a minimum 20 ms exposure of our camera. The slow penetration of antivortices (polarized against the polarity of the trapped flux) along the stripes is indicated by curved arrows in (c) and (e). Their gradual growth with H_a is clearly detected at each field. The TMAs nucleate at the bottom side, as in the case of the longitudinally polarized Py stripes (Fig.6), but less frequently. The major TMA trunks orient along the stripes and the branching occurs mostly near the middle of the sample, where the supercurrents invert.